Proceedings of the ASME 2023
International Design Engineering Technical Conferences and
Computers and Information in Engineering Conference
IDETC/CIE2023

August 20-23, 2023, Boston, Massachusetts

# DETC2023-114939

# NUMERICAL ANALYSIS AND WAVE TANK TEST OF A POINT ABSORBER WAVE ENERGY CONVERTER USING A TETHER DRIVEN POWER TAKE-OFF SYSTEM

Hu Zhang<sup>a</sup>, Liang Sun<sup>a</sup>, Jingxuan Liu<sup>b</sup>, Jia Mi<sup>c</sup>, Xiaofan Li<sup>c</sup>, Lin Xu<sup>a,d</sup>, Lei Zuo<sup>c\*</sup>

- a. School of Naval Architecture, Ocean and Energy Power Engineering, Wuhan University of Technology, Wuhan, China
- b. Hildebrand Department of Petroleum and Geosystems Engineering, University of Texas at Austin, TX, the United States
- c. Department of Naval Architecture and Marine Engineering, University of Michigan, MI, the United States
- d. School of Automotive Engineering, Wuhan University of Technology, Wuhan, China
- \*. Corresponding author: leizuo@umich.edu

#### **ABSTRACT**

Technologies to enhance the survivability of wave energy converters (WECs) in harsh ocean environment and reduce the difficulty and cost of deployment and operation are important. Traditional two-body point absorber with a rigid Power Take-off (PTO) may result in two essential problems on the deployment and operation. This study proposes a novel a two-body selfreactive point absorber with a flexible tether drive PTO. This flexible PTO design can avoid the request of supporting structures on the WEC to constrain the motion and harvest energy from multiple degree of freedoms (DOFs) motion without requirement of a taut mooring. System dynamics considering 4-DOF with the proposed flexible PTO system are formulated. A scaled prototype is designed, fabricated, and tested in a wave tank. Results show that the proposed flexible PTO can greatly increase the power absorption and add a reactive peak in the frequency domain. This study reveals that the proposed PTO is desirable for the two-body point absorber and thus holding the advantages of fast and easy deployment with slack mooring and good survivability under large wave conditions.

Keywords: Energy Harvesting; Wave Energy Converter; Power Take-off;

#### 1. INTRODUCTION

The world is having an increased demand for sustainable energy, and researchers have conducted exclusive study on different types of renewable energy[1]. Among different renewable energy sources, solar energy and wind energy are already widely used, and improvements are still being made on them[2][3][4][5]. For example, Hosseini and Wahid investigated photovoltaic-based hydrogen production and brought much attention[6]. Wen et al. conducted explicit study on the influence of the pitch and surge motion on power coefficient of the wind turbine, and the novel numerical method they used improved the calculating efficiency with good accuracy[7][8]. Ocean wave energy has attracted an increasing attention in recent years and many attempts have been made[9][10][11]. Unlike the wind energy, the ocean wave energy converters (WECs) can be classified into different categories based on their different forms and principles, for example, the overtopping device, the oscillating body device, and the oscillating water column, etc [12][13]. Among them, as suggested by Guo et al., the point absorber is one of the simplest, most broad-based, and most promising concepts where it just oscillate with the ocean wave to extract the kinetic energy from it [14]. In 1975, Budar raised the idea of a resonant single-body point absorber by implementing a flywheel to achieve efficiency ocean wave energy conversion [15]. One year later in 1976, Evans conducted analytical research on the single-body point absorber with various bodies [16]. Martin et al. proved that through design, the two-body point absorber can achieve better performance than the single-body point absorber[17], and explored the influence of different submerged body shapes [18]. Jin, Patton, and Guo optimized the geometry and damping coefficient of the point absorber, and significantly improved the power absorption by more than 70%[19]. Meng et al. systematically and thoroughly studied a submerged spherical point absorber and found out that significant efficiency improvement can be achieved through motion coupling[19], and by adjusting the mass distribution[21].

As the point absorber can be classified into a vibration energy harvester, nonlinearity can significantly influence the power absorption[22][23]. For example, Zhang et al. adopted bistable mechanism in the Power Take-off (PTO) of a point absorber and improved the power absorption bandwidth[24]. Liu et al. adopted the design in a winch-based PTO and achieved good improvement on the power absorption[25]. Li et al. designed a tunable flywheel that can be applied through semi-active control and achieved good result[26]. Jin et al introduced nonlinear stiffness into the breakwater and acquired satisfying improvement on wave attenuation and energy absorption performance simultaneously[27].

Inspired by the works mentioned above, in this research, we introduced a point absorber WEC with a unique tether drive PTO. The unique design of the PTO can avoid the request for supporting structures on the WEC and reduce the cost for deployment. In addition, the unique dynamic property of the one-way drive mechanism is discussed, Moreover, theoretical analysis is conducted to evaluate the performance of the proposed WEC and the advantages and disadvantages are introduced. At last, a scale model is fabricated and tested in the wave tank for validation.

#### 2. MATERIALS AND METHODS



Figure 1 The design of the proposed PTO

As illustrated in *Figure* 1, the torsional spring is locked with the main shaft and the floater to help retrieve the PTO back to the equilibrium position. The winch is fixed to the floater with one end of the tether, and the other end of the tether is connected

with the submerged reactive plate. The leaving relative motion between the floater and the submerged plate is adopted to pull the tether and drive the winch to rotate, and eventually drive the electromagnetic generator to generate electricity. The inertia of the generator and flywheel together formed an energy saving system. As a result, when the rotation speed of the generator and flywheel is faster than the drive speed of the winch, or when the tether is being retrieved, the kinetic energy saved in the flywheel will drive the generator and still output power. In such instances the PTO is decoupled into two parts, which are the input side and output side.

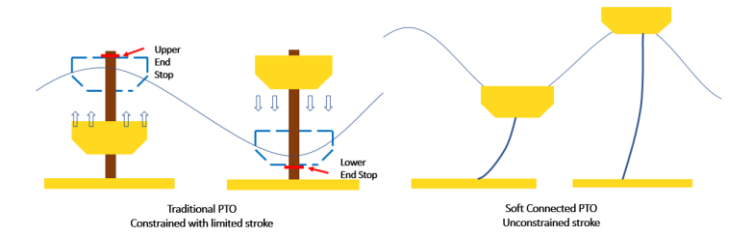


Figure 2 Comparison between the traditional linear drive PTO and the proposed soft drive PTO

The winch based soft connection design can bring in multiple advantages. Firstly, the soft connection design does not need to have a stroke limit, unlike the rigid connected PTOs that are constrained by the stroke length of the key component, for example the hydraulic cylinder, ballscrew, and linear generator, the soft connect can design the tether length based on the need of the users. Secondly, with such design, the entire PTO can be arranged inside the top floating buoy, which can provide better tightness and accessibility for maintenance. At last, the soft connection does not require rigid structure for linkage between the two bodies, which further improves the reliability and reduces the cost for the device as shown in Figure 2.

#### 3. RESULTS AND DISCUSSION

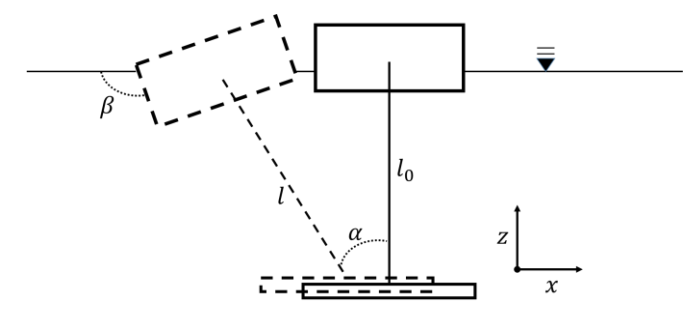


Figure 3 Scheme of the two-body configuration of the WEC with soft drive PTO

For the proposed device, usually three motions for each body are considered, which are the surge motion, heave motion

and the pitch motion. The influence of these three motions on the performance of the proposed WEC can be found in Figure 3, where l and  $l_0$  are the current and original length of the driving tether,  $\alpha$  is the angle of the tether between the heave direction, and  $(\beta - \frac{\pi}{2})$  is the pitching angle of the floating body.

The overall governing equation for the motion of the device can be described using the following equation,

$$\mathbf{M}\ddot{\mathbf{X}} = \mathbf{F}_e + \mathbf{F}_r + \mathbf{F}_h + \mathbf{F}_{pto} + \mathbf{F}_d + \mathbf{F}_m$$
Here  $\mathbf{M} = \begin{bmatrix} m_1 & 0 & 0 & 0 \\ 0 & m_2 & 0 & 0 \\ 0 & 0 & m_1 & 0 \\ 0 & 0 & 0 & m_2 \end{bmatrix}$ 

 $m_1$  and  $m_2$  are the mass of the floating and the submerged

body, and 
$$\mathbf{X} = \begin{bmatrix} x_1 \\ x_2 \\ z_1 \\ z_2 \end{bmatrix}$$
,  $x_1$  and  $x_2$  are the surge motion of the

floating and submerged body,  $z_1$  and  $z_2$  are the heave motion of the floating and submerged body. Similarly, the  $F_e$ ,  $F_r$ ,  $F_h$ ,  $F_{pto}$ ,  $F_d$  and  $F_m$ , are the vectors of excitation forces, radiation forces, hydrostatic forces, PTO induced forces, nonlinear drag forces, and mooring induced forces on the floating and submerged body in x and z directions.

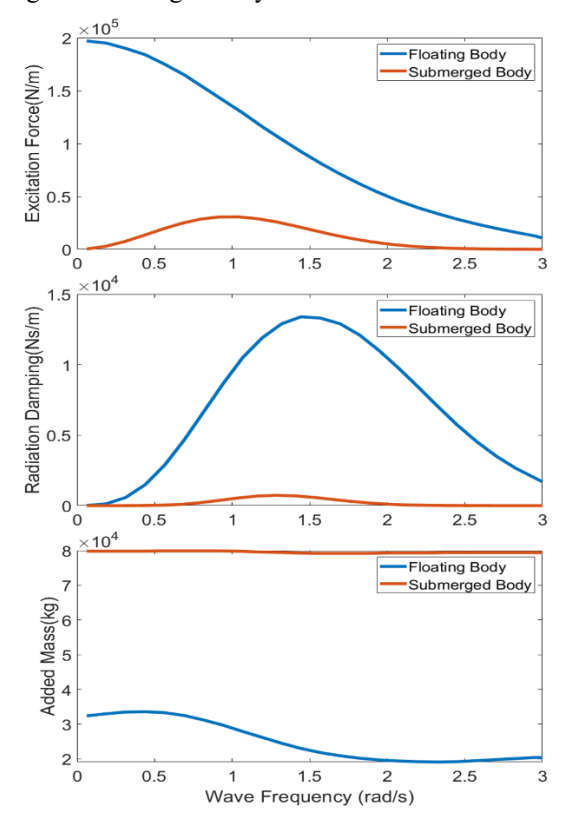


Figure 4 Hydrodynamic parameters for the floater and submerged body in heave motion

The frequency-dependent hydrodynamic parameters applied on the body can be calculated using the commercially available software AQWA and an example of the hydrodynamic parameters for the floater and submerged body in heave can be seen at Figure 4.

The radiation force is accounted by the added mass induced force and the radiation damping induced force, and the memory effect can be considered using the famous Cummins equation[28]:

The hydrostatic force applied to the body on the direction of the heave, meanwhile, since the submerged body don't have a section to interference with the free water surface[29]. The hydrostatic force applied to the submerged body becomes zero and the total representation of the hydrostatic force can be shown in the form of:

$$F_{h} = \begin{bmatrix} 0 \\ 0 \\ k_{hydro} z_{1} \\ 0 \end{bmatrix}$$
$$k_{hydro} = \rho g A_{h,1}$$

- $\rho$  is the density of the water
- g is the gravity constant
- A<sub>h\_1</sub> is the cross section area of the floater in heave motion

The PTO forces plays the most important role in the dynamic response and power absorption of the proposed WEC, and they can be presented as:

$$\boldsymbol{F_{pto}} = \begin{bmatrix} f_{pto,s} \\ -f_{pto,s} \\ f_{pto,h} \\ -f_{pto,h} \end{bmatrix}$$

•  $f_{pto,s}$  and  $f_{pto,h}$  are the PTO forces in the surge and heave directions

The design of the tether driving mechanism brings in several unique dynamic properties of the PTO that are worthy of discussion. Since the PTO is tether driven, the PTO force can only apply when the tether is in tension, which means that the PTO can only provide force in one direction. Moreover, the engagement and disengagement of the one-way clutch bring in the piecewise nonlinearity to the dynamics of the proposed PTO, and it needs to be expressed in different stages according to its working conditions.

As a result, a piecewise nonlinear equation can be used to describe the PTO force under the multi-stage working conditions in the surge direction:

$$\begin{split} f_{pto,s} \\ = \begin{cases} \left(-m_e \ddot{l} - c_e \dot{l} - k_e (l - l_0)\right) sin(\alpha), & l > l_0, \omega_w = \omega_g \\ \left(-k_e (l - l_0)\right) sin(\alpha), & l > l_0, \omega_w > \omega_g \\ 0, & l = l_0 \end{cases} \end{split}$$

Similarly, the equation for the PTO force in heave can also be derived as:

$$\begin{split} f_{pto,h} \\ &= \begin{cases} \left(-m_e \ddot{l} - c_e \dot{l} - k_e (l - l_0)\right) \cos(\alpha), & l > l_0, \omega_w = \omega_g \\ \left(-k_e (l - l_0)\right) \cos(\alpha), & l > l_0, \omega_w > \omega_g \\ 0, & l = l_0 \end{cases} \end{split}$$

- $m_e$  is the equivalent mass of the PTO[30]
- ullet  $c_e$  is the equivalent damping coefficient of the PTO
- $k_e$  is the equivalent spring stiffness of the PTO
- $\omega_w$  is the rotation speed of the winch
- $\omega_g$  is the rotation speed of the generator

The PTO will be separated into two subsystems that work independently, and the generator and flywheel side will be decoupled with the point absorber. The energy stored in the flywheel can continue to drive the PTO, and the speed of the generator will slowly decay exponentially, which can be expressed as:

$$\omega_q = \omega_{q \ 0} e^{-\frac{C_e}{m_e}t}$$

- $\omega_{g_0}$  is the rotation speed of the generator when the two subsystems decoupled
- *e* is the natural exponent

Here we define the decay factor  $r_{decay}$  as:

$$r_{decay} = -\frac{c_e}{m_e}$$

From the equation, it is easy to acquire that the generator speed decays faster with a smaller decay factor, which means either a larger damping coefficient or a smaller equivalent mass. It indicates the PTO nonlinearity is weaker and performs similarly to a linear PTO[31].

Since the analysis is to understand the fundamental of the PTO and provide guidance to the prototype design, some nonideal factors that have relatively small influence on the overall performance is ignored here, such as the friction terms from the mechanical systems, the cogging torque of the generator, and the stiffness from the components meshing, etc.

The drag force used in this paper is introduced as a quadratic damping term where it can be expressed as:

$$\mathbf{F}_{d} = \begin{bmatrix} f_{d,s_{-1}} \\ f_{d,s_{-2}} \\ f_{d,h_{-1}} \\ f_{d,h_{-2}} \end{bmatrix}$$

The drag force here is presented by the quadratic form and the drag coefficient used in this paper is estimated based on the body shape[29].

To study the influence of the mooring force, a simple spring force is adopted in both heave and surge motion on the floating and submerged body according to various arrangements of the mooring configurations, which can be written as:

$$\boldsymbol{F_m} = \begin{bmatrix} -k_{m,s\_1} x_1 \\ -k_{m,s\_2} x_2 \\ -k_{m,h\_1} z_1 \\ -k_{m,h\_2} z_2 \end{bmatrix}$$

The top of Figure 6 shows the PTO absorbed power for the proposed WEC under regular wave excitation where the wave height is 1m and the wave period is 6s. The dimension for the second body is 6m in diameter and placed 10m below the still water line. The unique dynamic property of the proposed tether-based PTO can be observed in the figure. Since the overall dynamics are highly nonlinear, the output power is irregular even under regular excitation conditions.

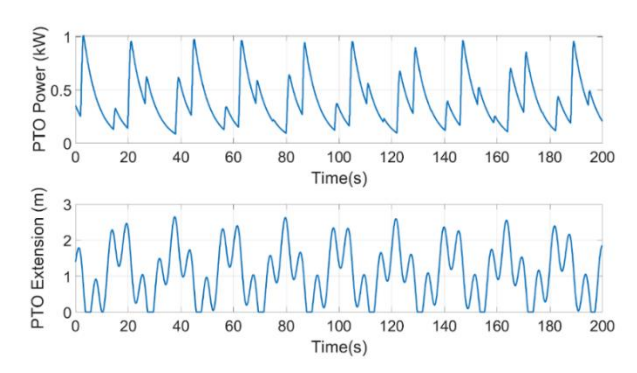


Figure 5 The time domain simulation results on the flexible tether drive PTO

The motion of the floating body and submerged body are illustrated in Figure 6. It can be observed from the figure that for the floating body, the surge and heave motion share similar strokes. However, the heave motion is the dominant motion for the submerged body. This is because the unique main drive direction of the tether on the submerged body is in heave, and the longer the distance between the two bodies, the smaller the drive

angle will be, which will finally lead to a dominant heave motion for the submerged body.

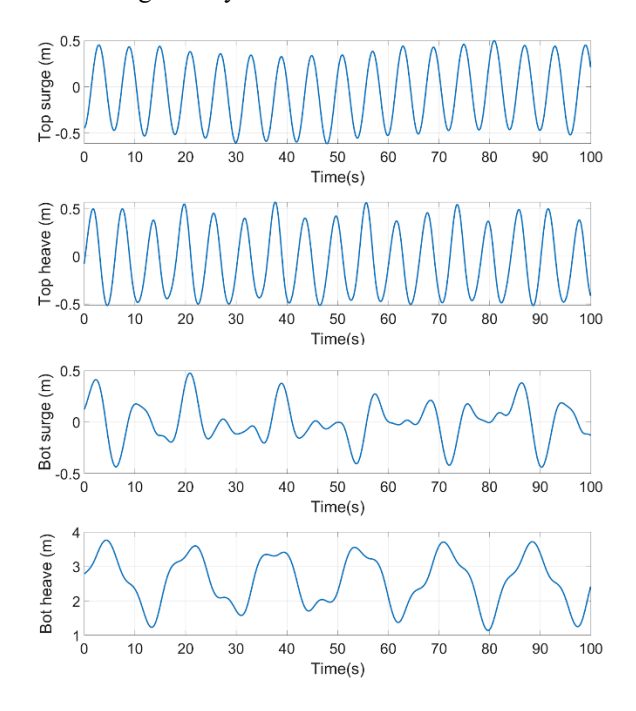


Figure 6 The motion of the two bodies under regular wave excitation

The PTO's free decay rate, when decoupled with the WEC, can be influenced by the ratio between the equivalent damping and the equivalent mass. Figure 7 shows the influence of the equivalent mass when other parameters for the WEC are the same. Due to the system's high nonlinearity, the result is selected to be in the same phase, yet the peak power varies greatly. The PTO damping is set as 5000Ns/m, and the spring stiffness is 5000N/m. It can be seen from the figure that the speed of the free decay decreases with the increase of the equivalent mass. The same damping coefficient indicates the same energy-consuming capability; when the equivalent mass is larger, more energy can be stored in the PTO under the same rotation speed. Thus, the energy dissipation rate is lower, which is reflected in the free decay rate.

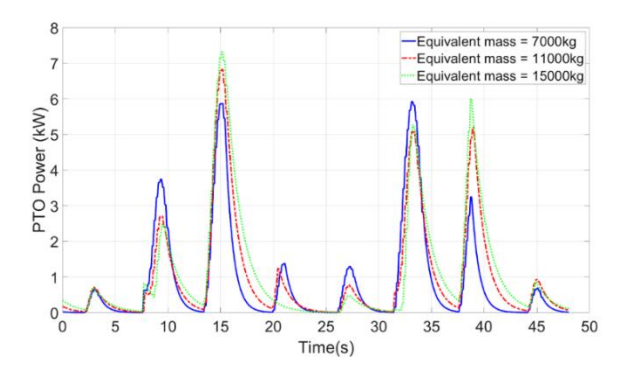


Figure 7 The influence of the equivalent mass of the PTO

Similarly, the equivalent damping can also influence the PTO characteristics. Figure 8 shows the influence of the different equivalent damping on the output power of the PTO. The selected equivalent mass is 15000kg, and the spring stiffness is 5000N/m. The increase of the equivalent damping can increase the energy-consuming capability. As a result, when stored energy in the flywheel is the same, the output power decreases faster for the PTO with a larger equivalent mass.

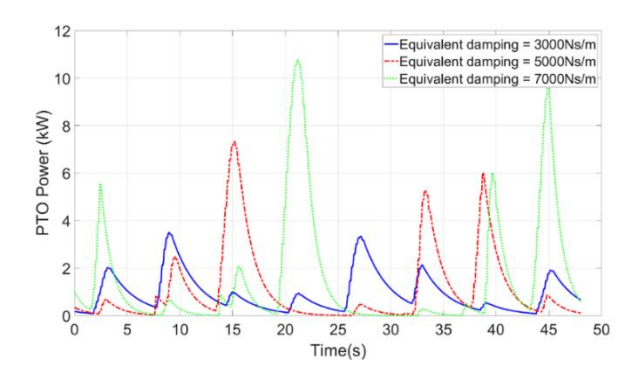


Figure 8 The influence of the damping coefficient of the PTO

From the previous figures, the PTO parameters can influence the performance of the WEC, and some situations are not preferred to exist in for the proposed WEC. For instance, Figure 9 shows two situations which are unfavorable. The first situation is when either the equivalent mass is too large or the equivalent damping is too small, the decay speed occupies multiple wave period and the power absorption from the ocean is limited, and it is shown in the left of Figure 9. The right side of Figure 9 illustrates another unfavorable condition where the equivalent mass of the PTO is too large that it take multiple waves to drive the flywheel. As a result, the tether also takes multiple wave periods to be recovered depending on the mooring configuration. Although the performance is different, both situations share the same issue where the energy from certain wave input is wasted, and can lead to either less power absorption or large peak to average ratio.

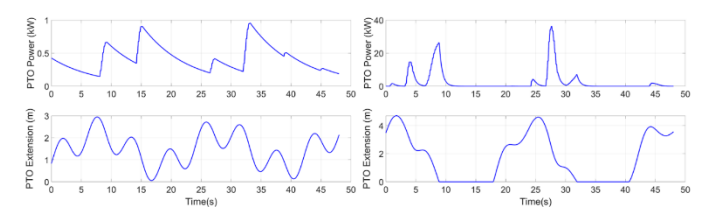


Figure 9 Two unfavorable conditions of the PTO under regular wave excitation

To avoid the high peak to average ratio that can damage the device and avoid the unfavorable situations, another two criteria are introduced in this research to establish a more comprehensive evaluation standard towards the performance of the proposed

device. One is the peak to average ratio of the power, the other is the disengaged time ratio. The peak to average ratio  $r_{pta}$  is denoted as:

$$r_{pta} = max(P_{pto})/avg(P_{pto})$$

Here,  $P_{pto}$  is the PTO absorbed power,

And the disengage ratio can be expressed as:

$$r_{dis} = \frac{total \; disengaged \; time}{total \; time}$$

In the study that follows, only the conditions that meet the two standards where  $r_{pta}$  smaller 15, and  $r_{dis}$  is smaller than 0.4 is used for further analysis.

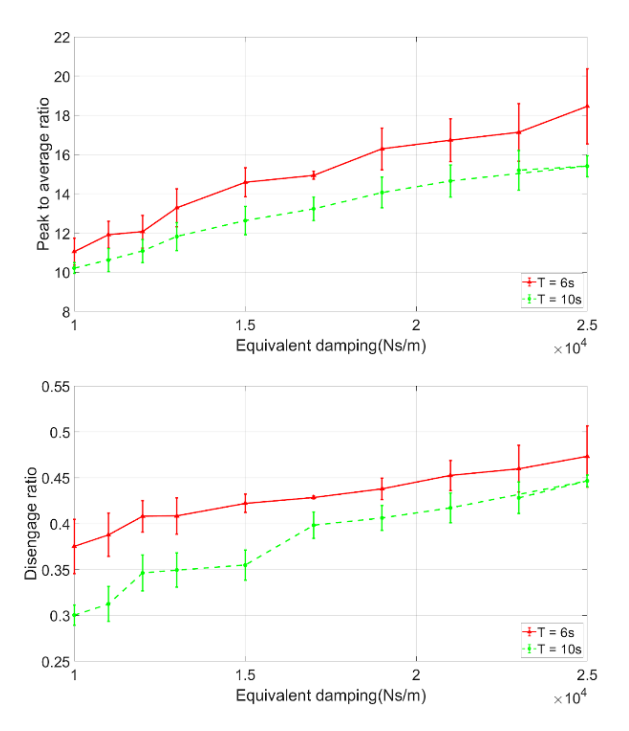


Figure 10 Peak to average ratio and disengage ratio of the PTO under different excitation conditions

The left side of Figure 10 shows the influence of the damping coefficient on the peak to average ratio, where the equivalent mass of the PTO is 10,000kg. The error bar shows the fluctuation due to the nonlinearity of the PTO. Each data point shows fifty groups of simulation with different initial conditions. From the figure, it can be observed that the equivalent damping can have large influence on the peak to average ratio. This reason for this phenomenon is already explained in the previous section, where the large equivalent damping can result in faster decay of the stored energy in the equivalent mass, and lead to larger disengage ratio, which will finally bring in a large peak to average ratio. The can also be verified through the figure on the right where the disengage ratio is presented.

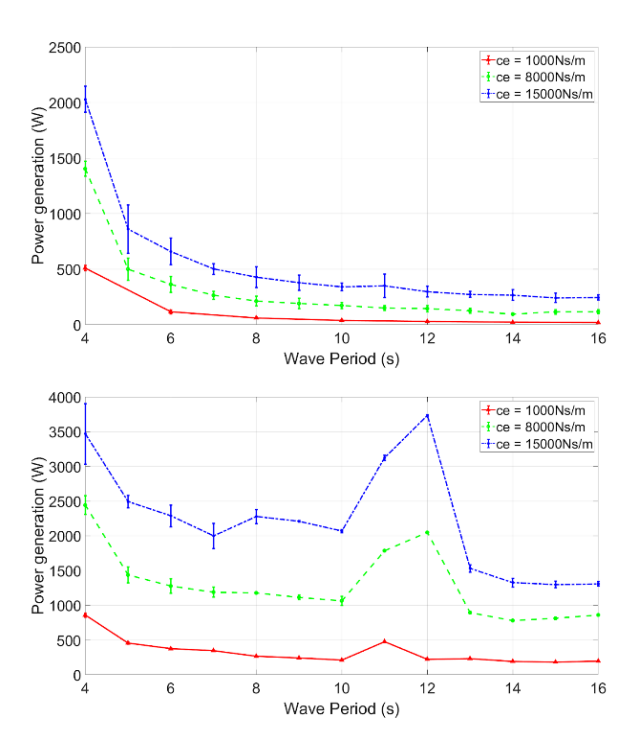


Figure 11 Compared results between the single-body and two-body configurations on the influence of the damping coefficient under different wave periods

The comparison between the single-body and two-body are introduced in Figure 11. The left side of Figure 11 shows the power absorption for a single-body point absorber with different damping from the PTO. From the figure, the two-body configuration can achieve better power absorption, for the two-body system can create another peak in the frequency domain by adding a reactive body. The position of the peak appeared in the two-body structure can be tuned by the adjusting the mass ratio between the surface body and the submerged body[32]. In addition, it can be seen that more power can be absorbed with larger damping coefficient, however, it also create larger peak to average ratio. As a result, the situations with larger damping coefficient is not introduced here.

The influence of the equivalent mass is shown in Figure 12. It can be observed that for both configurations, the influence of the equivalent mass is limited, yet it is more effective when the wave period is small. The two-body configuration can still achieve much better power generation performance than the single-body device on the discussed scale.

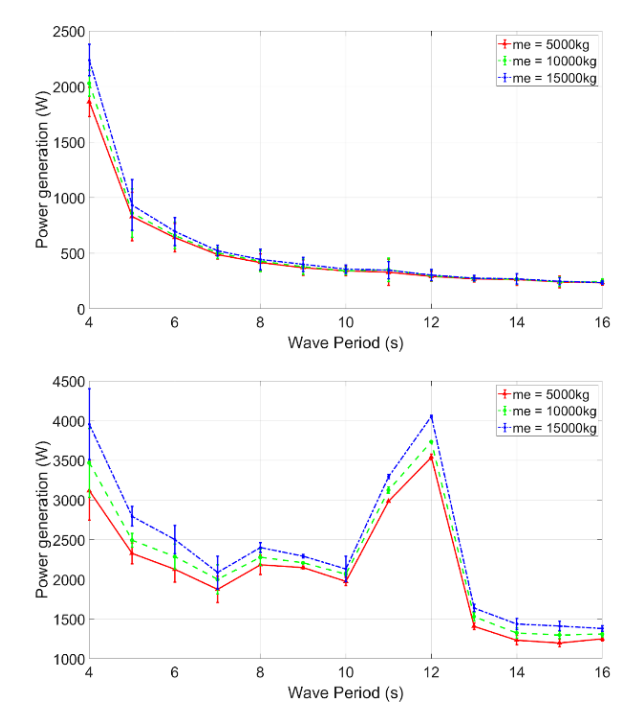


Figure 12 Compared results between the single-body and two-body configurations on the influence of the equivalent mass under different wave periods

#### 4. WAVE TANK VALIDATION

To verify the performance of the proposed device, a 1:10 scale prototype is fabricated and tested in the Wuhan University of Technology wave tank. The general test set-up can be seen in Figure 13. The overall dimension of the wave tank is 20m in length, 2.7 m in width, and 1m in depth. A hydraulic wave maker is used to generate waves based on the input requirement. Two wave probes are arranged at the front and back sides of the installation site to monitor the wave condition generated by the wave maker. The installation site is selected through an equilibrium process and located at the "sweet point" of the tank.

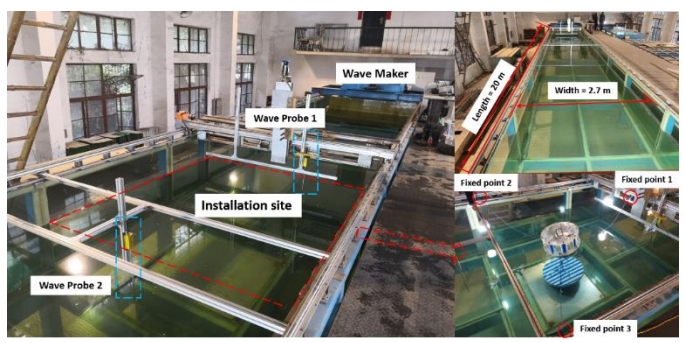


Figure 13 Wave tank test set-up

Figure 14 shows the time domain output from the wave tank test. The wave period used for the test is 1s, and the wave height is 0.09m. As suggested in the previous simulation section, the PTO's nonlinearity is strong where the single direction drive's unique phenomenon and the PTO's disengagement are apparent. In the test, a flywheel with relatively large inertia is assembled onto the PTO, and the external resistance is selected to be large to create a small PTO damping coefficient. As a result, the energy dissipation rate is slow, and the generator is always outputting power, where the peak to average ratio is reduced through such an approach.

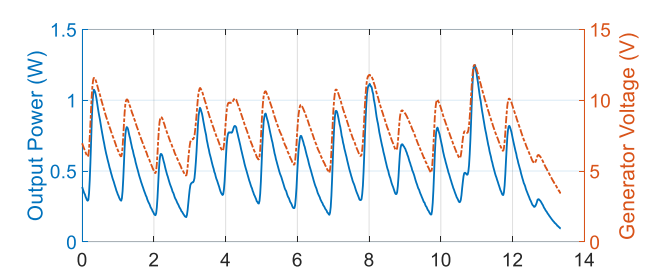


Figure 14 Time domain test results of the tested device under wave period of 1s and wave height of 0.09m

#### 5. CONCLUSION

In this paper, a novel PTO with soft connection by adopting a winch and rope mechanism is introduced. Such design can grant the system with multiple advantages for it can free the wave energy converter (WEC) from supporting structures and it can reduce the design constraint from key component. The dynamic modeling and numerical simulation for the PTO is accomplished. The results show that by selecting the key parameter of the damping coefficient and the equivalent mass of the PTO, it can always in the working condition where the rope is in extension. In addition, compared results show that by adding a reactive body, the WEC with the soft driven PTO can greatly increase the power absorption and adding a reactive peak in the frequency domain. The simulation is verified through the wave tark validation with a 1:10 scale prototype.

The unique dynamic characteristic of the PTO make it compatible with various working environment where it can be used with WEC, floating wind turbine, and wave gliders for additional power source. In future, the PTO design will be put into various working environment and optimize the power absorption based on different need to so the advantage of the design can be fully exploited.

## **ACKNOWLEDGEMENT**

The authors would like to sincerely acknowledge the support under the grant number of NSF 2246608.

### **REFERENCES**

- [1] Panwar, N. L., Kaushik, S. C., & Kothari, S. (2011). Role of renewable energy sources in environmental protection: A review. *Renewable and sustainable energy reviews*, 15(3), 1513-1524.
- [2] Herbert, G. J., Iniyan, S., Sreevalsan, E., & Rajapandian, S. (2007). A review of wind energy technologies. *Renewable and sustainable energy Reviews*, 11(6), 1117-1145.
- [3] Kannan, N., & Vakeesan, D. (2016). Solar energy for future world:-A review. *Renewable and sustainable energy reviews*, 62, 1092-1105.
- [4] Wen, B., Jiang, Z., Li, Z., Peng, Z., Dong, X., & Tian, X. (2022). On the aerodynamic loading effect of a model Spar-type floating wind turbine: An experimental study. *Renewable Energy*, 184, 306-319.
- [5] Wen, B., Li, Z., Jiang, Z., Tian, X., Dong, X., & Peng, Z. (2022). Floating wind turbine power performance incorporating equivalent turbulence intensity induced by floater oscillations. *Wind Energy*, 25(2), 260-280.
- [6] Hosseini, S. E., & Wahid, M. A. (2020). Hydrogen from solar energy, a clean energy carrier from a sustainable source of energy. *International Journal of Energy Research*, 44(6), 4110-4131.
- [7] Wen, B., Dong, X., Tian, X., Peng, Z., Zhang, W., & Wei, K. (2018). The power performance of an offshore floating wind turbine in platform pitching motion. *Energy*, 154, 508-521.
- [8] Wen, B., Tian, X., Dong, X., Li, Z., Peng, Z., Zhang, W., & Wei, K. (2020). Design approaches of performance-scaled rotor for wave basin model tests of floating wind turbines. *Renewable Energy*, 148, 573-584.
- [9] Chen, W., Lu, Y., Li, S., & Gao, F. (2023). A bioinspired foldable-wing wave energy converter for ocean robots. *Applied Energy*, 334, 120696.
- [10] Zheng, S., Phillips, J. W., Hann, M., & Greaves, D. (2023). Mathematical modelling of a floating Clam-type wave energy converter. *Renewable Energy*.
- [11] Gupta, A., & Tai, W. C. (2022). Ocean Wave Energy Conversion of a Spar Platform Using a Nonlinear Inerter Pendulum Vibration Absorber. In *International Design Engineering Technical Conferences and Computers and Information in Engineering Conference* (Vol. 86311, p. V010T10A013). American Society of Mechanical Engineers.

- [12] Antonio, F. D. O. (2010). Wave energy utilization: A review of the technologies. Renewable and sustainable energy reviews, 14(3), 899-918.
- [13] Guo, B., Wang, T., Jin, S., Duan, S., Yang, K., & Zhao, Y. (2022). A Review of Point Absorber Wave Energy Converters. *Journal of Marine Science and Engineering*, 10(10), 1534.
- [14] Al Shami, E., Zhang, R., & Wang, X. (2018). Point absorber wave energy harvesters: A review of recent developments. *Energies*, 12(1), 47.
- [15] Budar, K., & Falnes, J. (1975). A resonant point absorber of ocean-wave power. Nature, 256(5517), 478-479.
- [16] Evans, D. V. (1976). A theory for wave-power absorption by oscillating bodies. *Journal of Fluid Mechanics*, 77(1), 1-25.
- [17] Martin, D., Li, X., Chen, C. A., Thiagarajan, K., Ngo, K., Parker, R., & Zuo, L. (2020). Numerical analysis and wave tank validation on the optimal design of a two-body wave energy converter. *Renewable Energy*, *145*, 632-641.
- [18] Li, X., Liang, C., Chen, C. A., Xiong, Q., Parker, R. G., & Zuo, L. (2020). Optimum power analysis of a self-reactive wave energy point absorber with mechanically-driven power take-offs. *Energy*, 195, 116927.
- [19] Jin, S., Patton, R. J., & Guo, B. (2019). Enhancement of wave energy absorption efficiency via geometry and power take-off damping tuning. *Energy*, *169*, 819-832.
- [20] Meng, F., Ding, B., Cazzolato, B., & Arjomandi, M. (2019). Modal analysis of a submerged spherical point absorber with asymmetric mass distribution. *Renewable Energy*, 130, 223-237.
- [21] Meng, F., Rafiee, A., Ding, B., Cazzolato, B., & Arjomandi, M. (2020). Nonlinear hydrodynamics analysis of a submerged spherical point absorber with asymmetric mass distribution. *Renewable energy*, 147, 1895-1908.
- [22] Yang, T., Zhou, S., Fang, S., Qin, W., & Inman, D. J. (2021). Nonlinear vibration energy harvesting and vibration suppression technologies: Designs, analysis, and applications. *Applied Physics Reviews*, 8(3), 031317.
- [23] Zhang, X., Zhang, H., Zhou, X., & Sun, Z. (2022). Recent advances in wave energy converters based on nonlinear stiffness mechanisms. *Applied Mathematics and Mechanics*, 43(7), 1081-1108.
- [24] Zhang, X., Tian, X., Xiao, L., Li, X., & Lu, W. (2019). Mechanism and sensitivity for broadband energy harvesting of an adaptive bistable point absorber wave energy converter. *Energy*, *188*, 115984.

- [25] Liu, M., Bennett, A., Ruan, F., Li, X., Lou, J., Mi, J., & Zuo, L. (2022, August). A Self-Reactive Ocean Wave Energy Converter With Winch-Based Power Take-Off: Design, Prototype, and Experimental Evaluation. In International Design Engineering Technical Conferences and Computers and Information in Engineering Conference (Vol. 86311, p. V010T10A012). American Society of Mechanical Engineers.
- [26] Li, Q., Li, X., Mi, J., Jiang, B., Chen, S., & Zuo, L. (2020). Tunable wave energy converter using variable inertia flywheel. *IEEE Transactions on Sustainable Energy*, *12*(2), 1265-1274.
- [27] Jin, H., Zhang, H., Xu, D., Jun, D., & Ze, S. (2022). Low-frequency energy capture and water wave attenuation of a hybrid WEC-breakwater with nonlinear stiffness. *Renewable Energy*, 196, 1029-1047.
- [28] Cummins, W. E. (1962). The impulse response function and ship motions. David Taylor Model Basin Washington DC.
- [29] Chakrabarti, S. K. (1987). *Hydrodynamics of offshore structures*. WIT press.
- [30] Liu, M., Lin, R., Zhou, S., Yu, Y., Ishida, A., McGrath, M., ... & Zuo, L. (2018). Design, simulation and experiment of a novel high efficiency energy harvesting paver. *Applied energy*, 212, 966-975.
- [31] Li, X., Chen, C., Li, Q., Xu, L., Liang, C., Ngo, K., ... & Zuo, L. (2020). A compact mechanical power take-off for wave energy converters: Design, analysis, and test verification. *Applied Energy*, 278, 115459.
- [32] Liang, C., & Zuo, L. (2017). On the dynamics and design of a two-body wave energy converter. *Renewable energy*, 101, 265-274.